

Incommensurate magnetism in $K_2MnS_{2-x}Se_x$ and prospects for tunable frustration in a triangular lattice of pseudo-1D spin chains

Ankita Bhutani,¹ Piush Behera,¹ Rebecca D. McAuliffe,¹ Huibo Cao,² Ashfia Huq,² Melanie J. Kirkham,² Clarina dela Cruz,² Toby Woods,³ and Daniel P. Shoemaker¹

¹*Department of Materials Science and Engineering,
University of Illinois at Urbana-Champaign, Urbana, Illinois, USA.*

²*Neutron Scattering Division, Oak Ridge National Laboratory, Oak Ridge, TN 37831, United States*

³*School of Chemical Sciences, University of Illinois at Urbana-Champaign, Urbana, Illinois, USA.*

(Dated: March 10, 2022)

We report the first detailed investigation of K_2MnS_2 and K_2MnSe_2 from the K_2MnS_2 structure type and their magnetic solid solution $K_2MnS_{2-x}Se_x$ and find that compounds of this structure type consist of strongly-coupled pseudo-one-dimensional antiferromagnetic chains that collectively represent a frustrated two-dimensional triangular antiferromagnet. Bulk samples of $K_2MnS_{2-x}Se_x$ with $0 \leq x \leq 2$ are characterized using X-ray diffraction, neutron diffraction, magnetization and heat capacity measurements. An incommensurate cycloid magnetic structure with a magnetic propagation vector $k = [0.58 \ 0 \ 1]$ is observed for all samples in $K_2MnS_{2-x}Se_x$, and the ordering is robust despite a 12% increase in cell volume. Geometric frustration of chains results in incommensurability along a and a two-step magnetic transition. The varying geometries accessible in compounds of this structure type are presented as promising avenues to tune frustration.

I. INTRODUCTION

The rich physics in the magnetism of low dimensional and frustrated systems has been a topic of great interest since last 4-5 decades. [1, 2] Magnetic frustration, the competition of exchange couplings between localized spins, can be imposed by geometry or competing interactions and has broad implications for ground states and low-temperature properties. At low temperatures, peculiar behavior like spin ices [3] and spin liquids [2] can result when system fluctuates between different configurations or an ordered frustrated state with noncollinear and/or incommensurate magnetic structures can result with unsatisfied interactions in the Hamiltonian. [4, 5]

Within such systems, frustration can arise with different dimensionalities. Incommensurate magnetic ordering in quasi-1D magnetic systems can be caused by frustrated *intrachain* interactions as observed in $LiCuVO_4$, $NaCu_2O_2$, and $CuCl_2$, resulting in magnetic multiferroicity, [6–10] or it can be a hallmark of *interchain* magnetic interactions resulting from frustrated arrangements of chains as observed in triangular-lattice antiferromagnets (TLAFs) such as $CsNiCl_3$ and $Li_2NiW_2O_8$. [11]

In quasi-1D compounds, interchain coupling is required to induce long-range three-dimensional ordering (a Néel temperature) at finite temperatures. Exchange parameters J_{ij} can represent the “ideal” nearest-neighbor (nn) and next nearest-neighbor (nnn) intrachain spin-exchange couplings, here grouped as J_{intra} , while the longer-range interchain coupling between the chains is represented by J_{inter} . (Figure 1) Materials that approach the ideal 1-D Heisenberg limit would be those where the J_{intra} is strong but J_{inter} is weak; in this case 3D magnetic ordering may be highly degenerate, incommensurate, or not observed at all.

Identifying systems where exchange interactions are

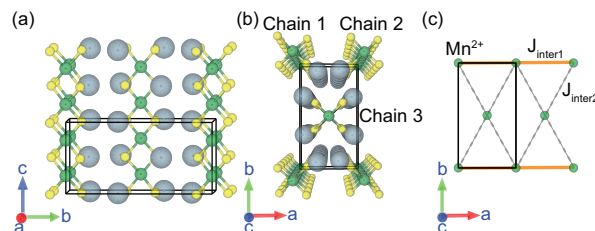


Figure 1. Crystal structure of 1D K_2MnS_2 and K_2MnSe_2 with views along a and c directions to show tetrahedrally coordinated Mn-Ch chains running along c . K^+ Mn^{2+} and chalcogen are represented by grey, green and yellow spheres respectively.

strong but frustrated is therefore of interest, with an additional benefit if the interactions are tunable and a range of spin and geometric constraints could be explored. K_2MnS_2 and K_2MnSe_2 belong to a rich family of quasi-1D compounds in the eponymous K_2MnS_2 structure type, where we concentrate on the representatives where A_2MX_2 , where $A = K, Na, Rb, Cs$; $M = Mn, Fe, Co, Zn, Si, Ge, Sn$; and $X = S, Se, Te, P, As$. K_2MnS_2 and K_2MnSe_2 were first synthesized by Bronger by the reaction of potassium carbonate with manganese in a stream of hydrogen charged with chalcogen.[12] Both these compounds exist in an orthorhombic space group $Ibam$ with edge-sharing $[MnX_4]^{-6}$ tetrahedral chains along the c direction. Viewed normal to the chains in Figure 1, the chain locations form isosceles triangles with their short distance along $\langle 100 \rangle$ and the long distance along $\langle 110 \rangle$.

The most closely-related compounds to the K_2MnS_2 structure type are the family of $AFeX_2$ ($A = K, Rb, Cs, Tl$; $X = S, Se$) compounds, which can be divided into three groups based on their crystal and magnetic structures. [13] All $AFeX_2$ compounds have tetrahedrally co-

ordinated Fe^{3+} chains along c , but many of these have an additional degree of structural freedom, manifested as a monoclinic distortion (TlFeS_2 , TlFeSe_2 , KFeSe_2 , and RbFeSe_2 with the magnetic moments ordered perpendicular to the chains; and KFeS_2 , RbFeS_2 with the ordered moments slightly tilted from the chain axis). [14, 15] Only CsFeS_2 is orthorhombic, but it further distorts martensitically at its magnetic transition at 70 K, with moments slightly tilted off the chain direction. [16]

Unlike the well-studied $A\text{FeX}_2$ -type compounds, the compounds in the A_2MX_2 family have not been examined in sufficient detail to understand any of their magnetic ground states. Only the compound K_2CoS_2 has been suggested to be a collinear antiferromagnet (on the basis of neutron diffraction by Bronger, but without any published data). [17] The antiferromagnetic nature of K_2MnS_2 and K_2MnSe_2 has been suggested based on susceptibility measurements. [12]

In this article, we present an investigation of the magnetic phase diagram of $\text{K}_2\text{MnS}_{2-x}\text{Se}_x$ using X-ray diffraction, neutron diffraction, magnetization and heat capacity measurements. This is the first detailed study of compounds from the family of A_2MCh_2 -type compounds. We propose an incommensurate antiferromagnetic structure for K_2MnS_2 using single crystal neutron diffraction and powder neutron diffraction caused by geometric frustration of chains. All compounds in the $\text{K}_2\text{MnS}_{2-x}\text{Se}_x$ series show similar magnetic ordering and T_N , and a two-step magnetic transition characteristic of TLAFs.

II. EXPERIMENTAL PROCEDURE

Bulk synthesis of the samples in the solid solution range of $\text{K}_2\text{MnS}_{2-x}\text{Se}_x$ with $0 \leq x \leq 2$ in increments of 0.2 was performed out using a solid state tube-in-a-tube method. Handling of reagents was performed in a glove box under argon. Reactions were conducted by loading S and Se in 15 mm diameter quartz tubes in their nominal composition. Metallic K spheres and Mn powder were loaded in a smaller tube resting inside the bigger tube. These tubes were then sealed under vacuum using liquid nitrogen and reacted in box furnaces at 600°C with a ramp rate of $1^\circ\text{C}/\text{min}$ and 48 h hold time, followed by furnace cooling. Synthesis of needle-shaped K_2MnS_2 single crystals was accomplished by high temperature gas flow, similar to the method reported by Bronger. [12] K_2CO_3 and Mn powder were mixed using a mortar and pestle in a stoichiometric ratio and reacted under an incoming 5% H_2/Ar stream charged with S vapor at 757°C .

Powder X-ray diffraction (XRD) measurements were conducted in transmission with a Bruker D8 diffractometer with $\text{Mo-K}\alpha$ radiation. Rietveld analysis on X-ray diffraction patterns was carried out using TOPAS 5. [18] All samples were pure as viewed by X-ray analysis except for the $x = 0.2$ sample.

Neutron powder diffraction (NPD) was performed in

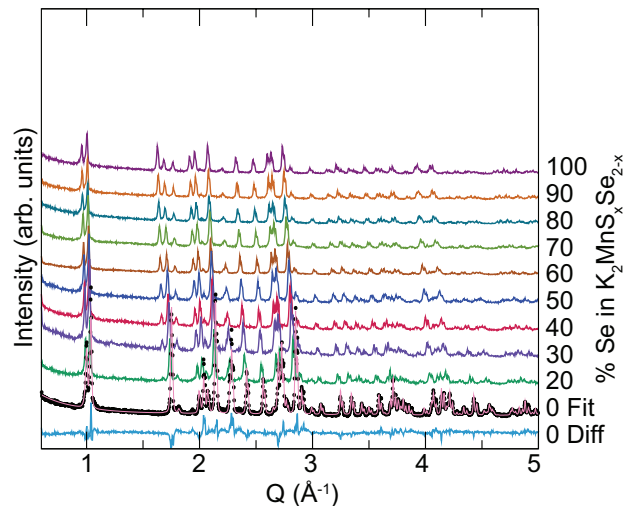


Figure 2. Laboratory X-ray diffraction patterns for $\text{K}_2\text{MnS}_{2-x}\text{Se}_x$ show consistent peaks for all samples, indicating a solid solution. The Rietveld refinement and difference curves for the K_2MnS_2 end member are shown at the bottom in pink and blue, respectively.

vanadium cans on the POWGEN instrument at the Spallation Neutron Source at Oak Ridge National Laboratory (ORNL). The temperature was raised from 10K to a maximum of 50K with a ramp rate of $0.5\text{K}/\text{min}$, and longer collections were taken at 10 K and 300 K. Processing and visualization of neutron powder diffraction data was done in the Mantid software. [19]

Single crystal neutron diffraction was collected for K_2MnS_2 on the HB-3A four-circle diffractometer at the High Flux Isotope Reactor at ORNL, with a neutron wavelength of 1.550 \AA selected from a bent perfect Si-220 monochromator. [20] The selected crystal had a size of $0.9 \times 0.2 \times 0.5 \text{ mm}$ and was sealed in a 0.7 mm diameter quartz tube (wall thickness 0.1 mm) to prevent air exposure. The crystal was held in place by another quartz capillary of 0.7 mm diameter. The tube was mounted on the cold head of the closed cycle refrigerator (CCR) to measure the temperature range from 4 K to 450 K. Data were collected at 4.0 K and the (020) and (060) Bragg peaks were measured at increasing temperatures. The nuclear and magnetic structure refinements and representation analysis are carried out with the FullProf Suite. [21] The magnetic symmetry analysis uses the Bilbao Crystallographic Server. [22–26]

Magnetic susceptibility measurements were collected on a Quantum Design MPMS3 magnetometer. Heat capacity measurements were performed using a Quantum Design Dynacool Physical Property Measurement System (PPMS).

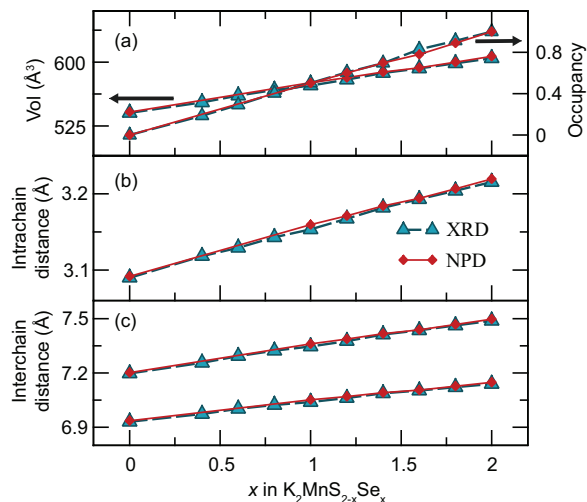


Figure 3. Across the solid solution from K_2MnS_2 to K_2MnSe_2 , Rietveld refinements to XRD and NPD data show smoothly varying cell volume (a), Se occupancy (a), intrachain Mn–Mn distance (c), and short and long interchain distances (d).

III. RESULTS AND DISCUSSIONS

A. Confirmation of solid solution behavior from X-ray and neutron diffraction

Rietveld refinements to laboratory powder X-ray diffraction show all synthesized compositions $\text{K}_2\text{MnS}_{2-x}\text{Se}_x$ except the $x = 0.2$ sample (Figure 2). Figure 3 shows the various refined structural parameters variation as a function of x in $\text{K}_2\text{MnS}_{2-x}\text{Se}_x$ for both laboratory XRD and NPD. The Se occupancy varies linearly with x , for both XRD and NPD. Across the whole composition range, increasing the Se content toward K_2MnSe_2 leads to a 12% volume increase. The difference in ionic radii of S (1.84 Å) and Se (1.98 Å) [27, 28] and increasing covalent nature with x causes an increase in Mn–S/Se bond length. The increase in volume is mirrored by an increase in Mn–Mn distances—both intrachain and interchain as shown in Figure 3 (b) and (c).

Figure 4(a,b) show the NPD patterns collected at 300 K and 10 K across the composition range of $\text{K}_2\text{MnS}_{2-x}\text{Se}_x$. The NPD data at 10 K show magnetic ordering in all compositions, with magnetic peaks that appear consistent across the compositional range, despite the large volume change and change in inter/intrachain distances. Surprisingly, the magnetic peaks could not be indexed to a commensurate k -vector, including the $[00\frac{1}{2}]$ ordering proposed for K_2CoS_2 by Bronger.[12]

Initial magnetic structure predictions using SARAH and FullProf suggested incommensurate ordering of the Mn^{2+} moments. Rough determination of T_N from NPD can be accomplished by noting the temperature of disappearance of magnetic peaks at $d = 5.2$ Å. Figure 5

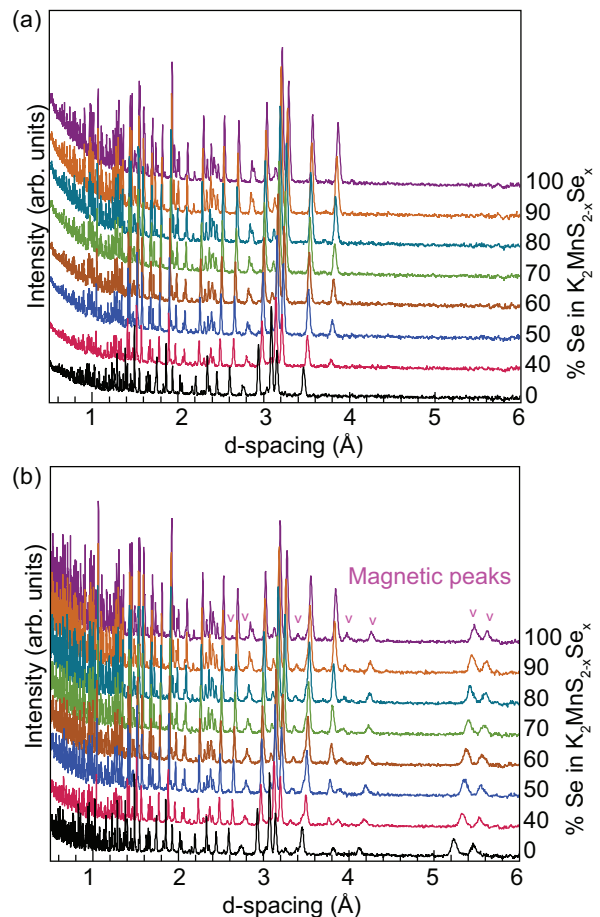


Figure 4. (a) Neutron powder diffraction patterns collected at (a) 300 K and (b) 4 K for $\text{K}_2\text{MnS}_{2-x}\text{Se}_x$. The 4 K data show magnetic peaks for all compositions marked with the pink pointers. The positions and intensities of the peaks portend equivalent magnetic ordering among the samples, but the propagation vector is incommensurate with the nuclear structure.

(a) and (b) show this range of NPD data for K_2MnS_2 and K_2MnSe_2 at $16 \pm 2\text{K}$ and $18 \pm 2\text{K}$ respectively. T_N for all compositions lie within in this temperature range and do not show a dramatic increase with x . This is despite the increasing distance between intrachain Mn1–Mn2 ions (4%), interchain Mn1–Mn3 ions (3%) and interchain Mn1–Mn4 ions (4%).

B. Incommensurate magnetic ordering in $\text{K}_2\text{MnS}_{2-x}\text{Se}_x$

Magnetic reflections appear below $T = 17\text{K}$ for all compositions in $\text{K}_2\text{MnS}_{2-x}\text{Se}_x$ as shown in Figure 5(a,b). An order parameter plot for is shown in Figure 5(c) from single crystal neutron diffraction of K_2MnS_2 . The presence of magnetic reflections in both single crystal and powder neutron diffraction is consistent with our magnetic susceptibility and heat capacity measurements. The mag-

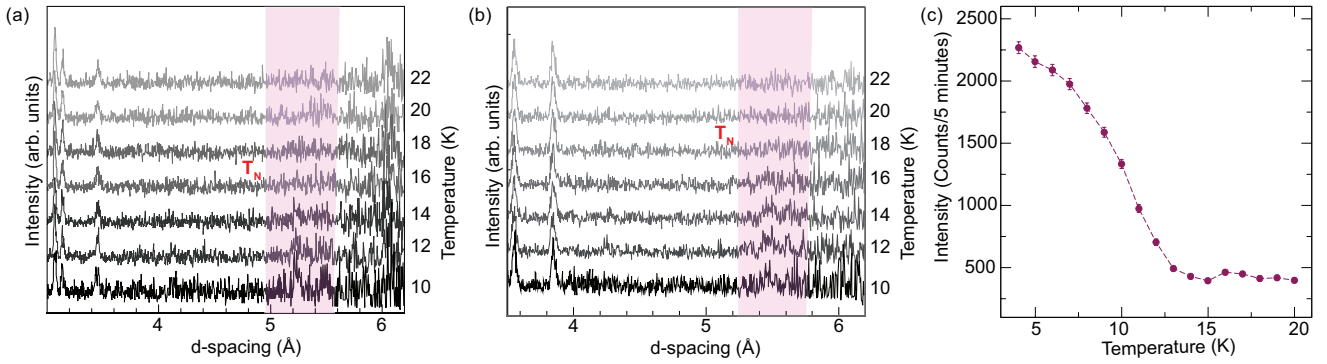


Figure 5. NPD with increasing T shows disappearance of the magnetic peaks around 15 K for (a) K_2MnS_2 and (b) K_2MnSe_2 , while triple-axis single-crystal intensity on the (0.4211) peak (c) provides a more precise view of the order parameter evolution. The exact temperature is best judged by heat capacity measurements.

netic phase was indexed using an incommensurate magnetic propagation vector $k = [0.58 \ 0 \ 1]$ at 4 K. The final refinement of single crystal neutron diffraction data is shown in Figure 6 where the observed and calculated structure factors for the nuclear and magnetic refinements are plotted. The refined magnetic structure results in a cycloidal configuration of magnetic moments in the ab plane as shown in Figure 7. The spins are antiferromagnetically coupled along the chains in the c direction. The total refined magnetic moment is $2.279 \mu_B$, considerably smaller than $5.92 \mu_B$ expected for Mn^{2+} ($S = 5/2$). A reduced magnetic moment is often observed in quasi-1D spin systems such as $\text{NaFeGe}_2\text{O}_6$, Na_2TiCl_4 and has been believed to be caused by spin fluctuations and covalency.[29, 30] Delocalization of d electrons could be another explanation for reduced magnetic moment as observed in RbFeSe_2 . [13] Here, it is more likely that the reduced moment arises from latent disorder due to the

frustrated moments in K_2MnS_2 . Accordingly, the steady increase of the magnetic peak (0.42 1 1) order parameter upon cooling to 4 K indicates that the magnetic ordering is not complete. (Figure 5 (c)) Magnetic refinements to the NPD data at 10 K confirm that the cycloid model can be assumed as the magnetic structure for the full substitution range (Figure 4). However, a very good fit for the powder intensity at $d = 5.23 \text{ \AA}$ could not be obtained.

The spin lattice in K_2MnS_2 and K_2MnSe_2 is comprised of isosceles triangles, with two nearest-neighbor ($J_{\text{inter}1}$) and four next-nearest-neighbor interactions ($J_{\text{inter}2}$) as shown in Figure 1(c). The relative strengths of inter-chain exchange interactions $J_{\text{inter}1}$ and $J_{\text{inter}2}$, and J_{intra} and anisotropy terms in the Hamiltonian determine the final magnetic ordering of the system. Such a triangular lattice can form a simple non-frustrated square lattice if $J_{\text{inter}1} = 0$ and $J_{\text{inter}2} \neq 0$, a strongly frustrated triangular lattice if $J_{\text{inter}1} \approx J_{\text{inter}2} \neq 0$, and a decoupled spin chain if $J_{\text{inter}1} \neq 0$ and $J_{\text{inter}2} = 0$. Overall, the

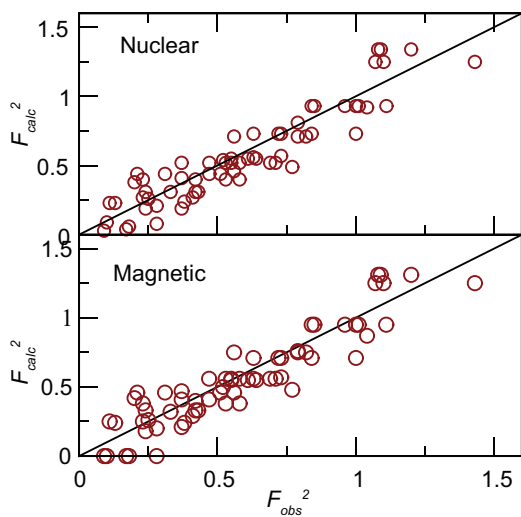


Figure 6. Calculated vs observed structure factors for nuclear and magnetic reflections obtained from single crystal neutron diffraction refinement of K_2MnS_2

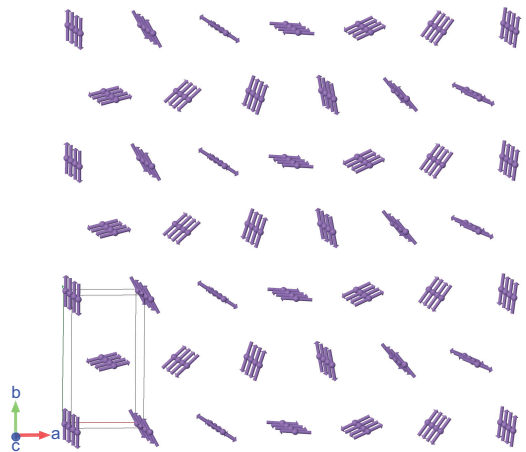


Figure 7. Magnetic structure of K_2MnS_2 determined from single crystal neutron diffraction showing the cycloid arrangement of spins in the ab plane with incommensurability along a direction.

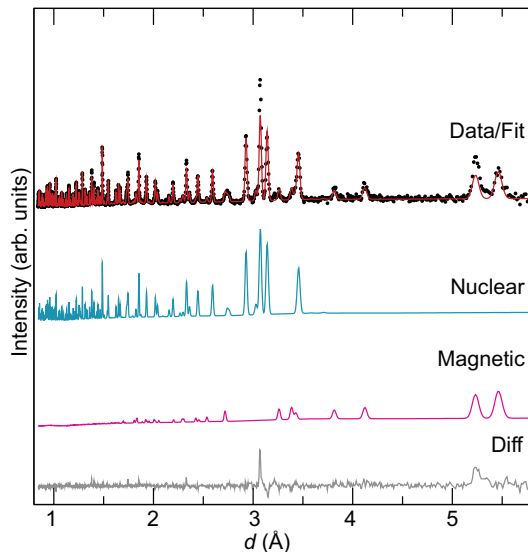


Figure 8. Rietveld refinement of neutron powder diffraction data of K_2MnS_2 collected at 10K with $k = [0.58 \ 0 \ 1]$.

magnetic frustration in K_2MnS_2 manifests itself in the form of incommensurability along a direction. A similar ground state to K_2MnS_2 is seen in the frustrated quasi-1D triangular lattice antiferromagnetic systems CsNiCl_3 , CsCoCl_3 , $\text{NaFeGe}_2\text{O}_6$, [29] and $\text{Li}_2\text{NiW}_2\text{O}_8$. [11] In the case of $\text{Li}_2\text{NiW}_2\text{O}_8$, strong anisotropy can overcome the effect of frustration and stabilize a collinear magnetic order. Collinear magnetic structures are also observed in monoclinic compounds, where the unique angle β removes the interchain frustration, as seen in TlFeS_2 and TlFeSe_2 . [31] Comparison of neutron powder diffraction patterns for $\text{K}_2\text{MnS}_{2-x}\text{Se}_x$ compounds from Figure 4 reveal similar magnetic ordering in all compositions and the cycloid model is proposed as the magnetic structure in these compounds.

C. Similar T_N in $\text{K}_2\text{MnS}_{2-x}\text{Se}_x$

The determination of T_N is more precise in these compounds when viewed by magnetic susceptibility, single-crystal neutron diffraction, and heat capacity. Magnetic susceptibility measurements for $x = 0.0, 1.0$ and 1.8 are displayed in Figure 9. The magnetic susceptibilities of quasi-1D magnets exhibit two characteristic maxima: a broad maximum at high temperatures associated with the short-range intrachain order in 1D, and a sharper kink at low-temperatures associated with the interchain transition into a 3D magnetically ordered phase. The 3D-ordering peak (T_N) appears at ~ 17 K for $x = 0, 1$ and 1.8 . However, our susceptibility measurements up to 300 K do not approach the region of maximum susceptibility due to intrachain coupling, as is typical for related systems with strong 1-D order: KFeS_2 and CsFeS_2 display maxima at $T = 565$ and 800 K, respectively.

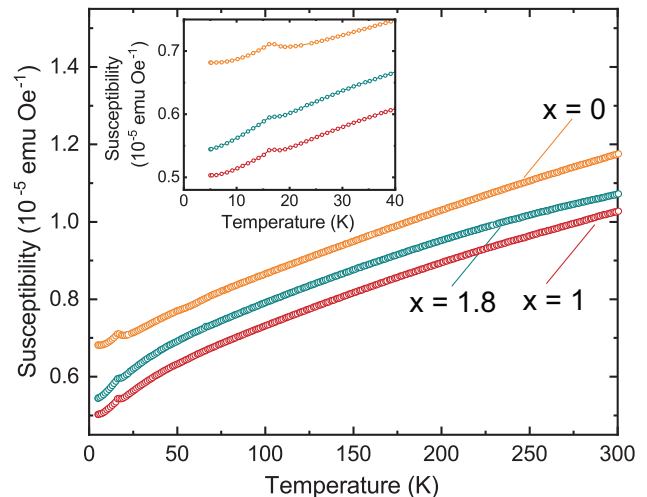


Figure 9. Magnetic susceptibility for three different compositions in $\text{K}_2\text{MnS}_{2-x}\text{Se}_x$

[32] Other compounds, such as TlFeS_2 , TlFeSe_2 , and RbFeSe_2 , show a linear increase in susceptibility above T_N and no signs of saturation, which may arise from delocalization of d electrons due to small intrachain Fe-Fe distances. A small degree of itinerancy and hence one-dimensional metallic behavior is expected but has never been shown in these ternary iron chalcogenides. Difficulties in handling such fragile, fiber-like crystals and the presence of defects and mechanical breaks in the crystals complicate verification of the metallic nature at a microscopic level. [13, 31] A linear increase in susceptibility has also been observed in two-dimensional metallic layered iron pnictides in the paramagnetic regime, which may arise from the tendency to exhibit moments that have mixed local and itinerant character.[33] The Mn^{2+} - Mn^{2+} distance is ~ 3.1 Å in K_2MnS_2 while the shortest Mn-Mn distance in metallic manganese is 2.67 Å, so some degree of itinerancy can be expected in K_2MnS_2 and K_2MnSe_2 .

In the absence of high-temperature susceptibility data showing the broad maximum and paramagnetic behavior following the Curie-Weiss law, existing models for 1D magnetic chains such as the Wagner-Friedberg model, the Rushbrooke-Wood model, the Emori model cannot be used to estimate the value of intrachain coupling as in KFeS_2 and CsFeS_2 . [34–36] If we assume very small degree of itinerancy in K_2MnS_2 and K_2MnSe_2 and that they reach a maximum at higher temperature, results compiled by De Jongh and Miedema can be used to put a lower bound on intrachain coupling constant J using $T_{\text{max}}/J \approx 10.6$, giving $J_{\text{intra}} > 28$ K since $T_{\text{max}} > 300$ K. [37]

J_{intra} is governed by the direct and super-exchange interactions between Mn^{2+} - Mn^{2+} while J_{inter} , on the other hand, is governed by complicated super-super exchange interactions via Mn-S/Se..S/Se-Mn pathways. While the direct exchange is only governed by distance between

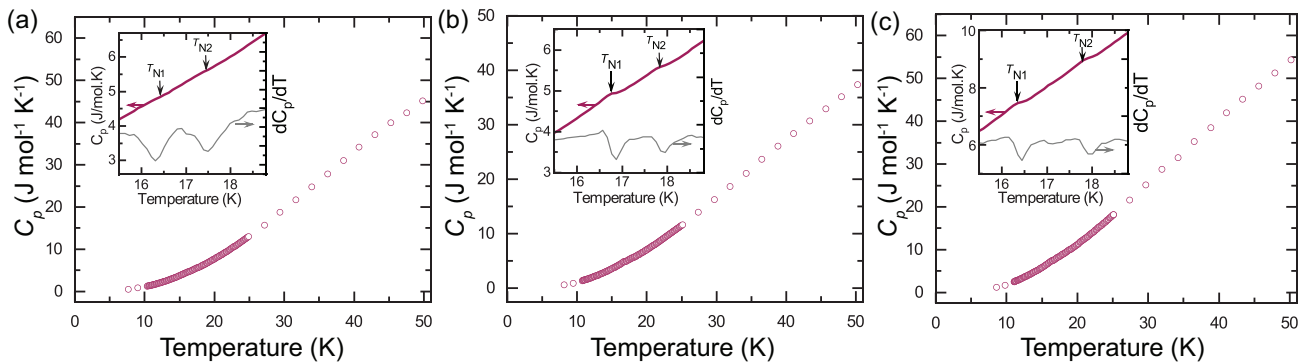


Figure 10. Heat capacity data for samples with $x = 0, 1,$ and 1.8 in $\text{K}_2\text{MnS}_{2-x}\text{Se}_x$ (a-c, respectively) show two closely-spaced transitions, likely corresponding to an initial interchain ordering along the shortest direction (a axis), followed by full 3D ordering.

$\text{Mn}^{2+}\text{-Mn}^{2+}$, the higher levels of exchange interactions depend on two opposing factors: the geometric effect of a larger bridging anion (Se) causing an increase in $\text{Mn}^{2+}\text{-Mn}^{2+}$ distance, and decrease in polarizability of the bridging anion. The final magnetic ordering temperature T_N can be conjectured based on the degree of frustration that arises from the relative strengths of $J_{\text{inter}1}$ versus $J_{\text{inter}2}$, J_{intra} and anisotropy terms in the Hamiltonian. The balance between these complex terms is surprisingly robust in the case of $\text{K}_2\text{MnS}_{2-x}\text{Se}_x$, since there is no discernible change in T_N across the substitution range.

D. Signature of a two-step magnetic transition in $\text{K}_2\text{MnS}_{2-x}\text{Se}_x$

Heat capacity data measured for $x = 0, 1, 1.8$ are shown in Figure 10 from $T = 6$ K to 45 K. Two transitions at 16 and 18 K can be observed in all three samples, most easily seen in the first temperature derivatives dC_p/dT . Neutron diffraction confirms that at least one of these transitions is magnetic in nature, but they likely correspond to two consecutive magnetic orderings. The frustration or competition between $J_{\text{inter}1}$ and $J_{\text{inter}2}$ with anisotropy is typically invoked to explain the splitting of T_N into two, as observed in ABX_3 -type compounds, and is relevant here.[38] In such a case, increasing the applied magnetic field should cause the two transitions to merge, which we observed in K_2MnS_2 at $H = 5$ T. (Figure S1) This consecutive-ordering case is more likely than two-step magnetic transitions in quasi-1D compounds from ordering of magnetic ions at inequivalent crystallographic sites (all Mn sites are equivalent here),[39] or an accompanying structural transition (as in BaFe_2As_2).[40] A two-step transition could not be observed in magnetic susceptibility measurements (Figure 9) because the peak in susceptibility is relatively broad, with $\text{FWHM} > 2$ K compared to the ~ 1.5 K spacing between the various T_{N1} and T_{N2} . Further measurements probing magnetic

states between T_{N1} and T_{N2} can fully shed light on the evolution of magnetic orderings with temperature exhibited by these compounds.

E. Interchain anisotropy across many compounds in the K_2MnS_2 structure type

There are about 30 compounds of the type A_2MX_2 in the *Ibam* K_2MnS_2 structure type reported in the Inorganic Crystal Structure Database. [41] Those with Mn, Co, Fe can be assumed to be magnetic, while others where $M = \text{Zn}, \text{Si}, \text{Ge}, \text{Sn}$ are not. As an arena for tuning magnetic interactions, intrachain couplings can produce systems that are frustrated along one direction, for exam-

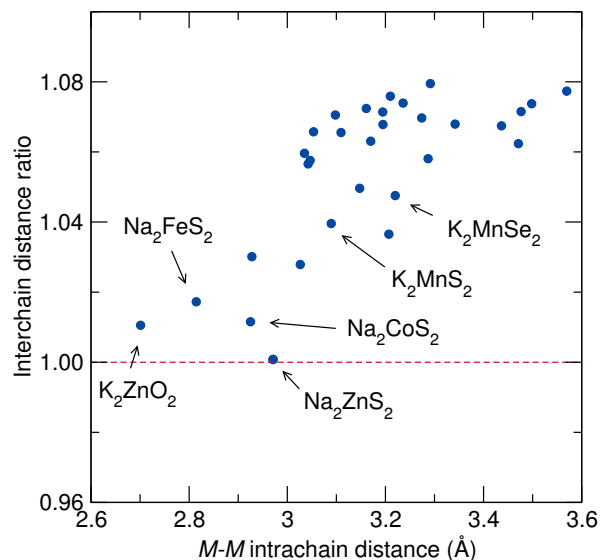


Figure 11. Ratio of the long versus short interchain distances versus the intrachain metal-metal distance for all members of the K_2MnS_2 structure type where M is a cation. Compounds where the ratio = 1 have 1-D chains that lie on a nearly perfect triangular lattice.

ple in LiCuVO_4 , NaCu_2O_2 , and CuCl_2 , [6–10] while separately, these chains interact on a triangular lattice which we show to have much weaker (< 1000 times) interactions. In the $\text{K}_2\text{MnS}_{2-x}\text{Se}_x$ system, the triangular lattice is anisotropic, made of isosceles triangles where the long distance is approximately 4% longer than the short distance. In the interest of tuning these distances to further frustrate the system, an ideal triangular lattice would occur when the two distances are equal. At this point we believe that the interchain ordering could be further suppressed, below the ~ 17 K temperatures seen here. In Figure 11, we plot the ratio of the long versus short interchain distance for all known A_2MX_2 compounds, along with the M - M intrachain distance. The only compound that has been examined by neutron diffraction is K_2CoS_2 , which Bronger and Bomba noted as an antiferromagnet with $T_N > 9.5$ K, but no data or metrics were included to evaluate the structure solution.[12] Their proposed model included Co moments pointing along the intrachain direction, so there are clearly many degrees of freedom that remain unexplored in this diverse system, and the full list of compounds with distances in ratios is given in Table S1.

IV. SUMMARY AND OUTLOOK

In summary, we have presented the first detailed investigation of K_2MnS_2 and K_2MnSe_2 compounds from their

eponymous structure type and their magnetic solid solution $\text{K}_2\text{MnS}_{2-x}\text{Se}_x$. We observe an incommensurate cycloid magnetic structure for all samples in $\text{K}_2\text{MnS}_{2-x}\text{Se}_x$, identified by single crystal neutron diffraction of K_2MnS_2 at 4 K and powder neutron diffraction of all samples at 10 and 50 K. The quasi-1D compound is best represented as a 2D triangular antiferromagnet, which results in geometric frustration of chains resulting in incommensurability along a , a two-step magnetic transition characteristic of differing $J_{\text{inter}1}$ and $J_{\text{inter}2}$, and the prospect for tuning these interactions via a wide array of substitution in isostructural compounds.

ACKNOWLEDGMENTS

We acknowledge support from the Center for Emergent Superconductivity, an Energy Frontier Research Center funded by the U.S. Department of Energy, Office of Science, Office of Basic Energy Sciences under Award Number DEAC0298CH1088. Characterization was performed in the Materials Research Laboratory Central Research Facilities, University of Illinois. Single crystal neutron diffraction and powder neutron diffraction were conducted at ORNL’s High Flux Isotope Reactor and Spallation Neutron Source, sponsored by the Scientific User Facilities Division, Office of Basic Energy Sciences, U.S. Department of Energy.

-
- [1] A. Ramirez, *Ann. Rev. Mater. Sci* **24**, 453 (1994).
 - [2] L. Balents, *Nature* **464**, 199 (2010).
 - [3] S. T. Bramwell and M. J. Gingras, *Science* **294**, 1495 (2001).
 - [4] H. Nakamura, T. Yamasaki, S. Giri, H. Imai, M. Shiga, K. Kojima, M. Nishi, K. Kakurai, and N. Metoki, *J. Phys. Soc. Japan* **69**, 2763 (2000).
 - [5] V. Kiryukhin, Y. Kim, K. Thomas, F. Chou, R. Erwin, Q. Huang, M. Kastner, and R. Birgeneau, *Phys. Rev. B* **63**, 144418 (2001).
 - [6] B. Gibson, R. Kremer, A. Prokofiev, W. Assmus, and G. McIntyre, *Physica B* **350**, E253 (2004).
 - [7] L. Capogna, M. Mayr, P. Horsch, M. Raichle, R. Kremer, M. Sofin, A. Maljuk, M. Jansen, and B. Keimer, *Phys. Rev. B* **71**, 140402 (2005).
 - [8] M. Banks, R. Kremer, C. Hoch, A. Simon, B. Ouladdiaf, J.-M. Broto, H. Rakoto, C. Lee, and M.-H. Whangbo, *Phys. Rev. B* **80**, 024404 (2009).
 - [9] L. Capogna, M. Reehuis, A. Maljuk, R. Kremer, B. Ouladdiaf, M. Jansen, and B. Keimer, *Phys. Rev. B* **82**, 014407 (2010).
 - [10] M. Mourigal, M. Enderle, R. K. Kremer, J. M. Law, and B. Fåk, *Phys. Rev. B* **83**, 100409 (2011).
 - [11] K. Ranjith, R. Nath, M. Majumder, D. Kasinathan, M. Skoulatos, L. Keller, Y. Skourski, M. Baenitz, and A. Tsirlin, *Phys. Rev. B* **94**, 014415 (2016).
 - [12] W. Bronger, H. Balk-Hardtdegen, and D. Schmitz, *Z. Anorg. Allg. Chem.* **574**, 99 (1989).
 - [13] Z. Seidov, H.-A. K. von Nidda, V. Tsurkan, I. Filipova, A. Günther, T. Gavrilova, F. Vagizov, A. Kiiamov, L. Tagirov, and A. Loidl, *Phys. Rev. B* **94**, 134414 (2016).
 - [14] E. Asgerov, N. Dang, A. Beskrovnyy, A. Madadzada, D. Ismayilov, R. Mehdiyeva, S. Jabarov, and E. Karimova, *Semiconduct.* **49**, 879 (2015).
 - [15] W. Bronger, A. Kyas, and P. Müller, *J. Solid State Chem.* **70**, 262 (1987).
 - [16] M. Nishi, Y. Ito, and A. Ito, *J. Phys. Soc. Japan* **52**, 3602 (1983).
 - [17] W. Bronger and C. Bomba, *J. Less-Common Met.* **158**, 169 (1990).
 - [18] A. A. Coelho, *A Computer Programme for Rietveld Analysis* (2004).
 - [19] O. Arnold, J.-C. Bilheux, J. Borreguero, A. Buts, S. I. Campbell, L. Chapon, M. Doucet, N. Draper, R. F. Leal, M. Gigg, *et al.*, *Nuclear Instruments and Methods in Physics Research Section A: Accelerators, Spectrometers, Detectors and Associated Equipment* **764**, 156 (2014).
 - [20] B. C. Chakoumakos, H. Cao, F. Ye, A. D. Stoica, M. Popovici, M. Sundaram, W. Zhou, J. S. Hicks, G. W. Lynn, and R. A. Riedel, *J. Appl. Cryst.* **44**, 655 (2011).
 - [21] J. Rodriguez-Carvajal, in *Satellite Meeting on Powder Diffraction of the XV Congress of the IUCr*, Vol. 127 (Toulouse, France:[sn], 1990).
 - [22] M. I. Aroyo, J. M. Perez-Mato, C. Capillas, E. Kroumova, S. Ivantchev, G. Madariaga, A. Kirov, and H. Won-

- dratschek, *Z. Kristall.* **221** (2006).
- [23] M. I. Aroyo, A. Kirov, C. Capillas, J. M. Perez-Mato, and H. Wondratschek, *Acta Cryst. A* **62**, 115 (2006).
- [24] M. Aroyo, J. Perez-Mato, D. Orobengoa, E. Tasci, G. De La Flor, and A. Kirov, *Bulg. Chem. Commun.* **43**, 183 (2011).
- [25] S. V. Gallego, E. S. Tasci, G. de la Flor, J. M. Perez-Mato, and M. I. Aroyo, *J. Appl. Cryst.* **45**, 1236 (2012).
- [26] J. Perez-Mato, S. Gallego, E. Tasci, L. Elcoro, G. de la Flor, and M. Aroyo, *Ann. Rev. Mater. Res.* **45**, 217 (2015).
- [27] R. T. Shannon and C. T. Prewitt, *Acta Cryst. B* **25**, 925 (1969).
- [28] R. T. Shannon and C. Prewitt, *Acta Cryst. B* **26**, 1046 (1970).
- [29] L. Ding, P. Manuel, D. D. Khalyavin, F. Orlandi, and A. A. Tsirlin, *Phys. Rev. B* **98**, 094416 (2018).
- [30] M. Winkelmann, D. Welz, M. Baehr, D. Hinz, T. Dedecke, W. Urland, and G. Meyer, *J. Magn. Magn. Mater.* **140**, 1667 (1995).
- [31] Z. Seidov, H.-A. K. von Nidda, J. Hemberger, A. Loidl, G. Sultanov, E. Kerimova, and A. Panfilov, *Phys. Rev. B* **65**, 014433 (2001).
- [32] S. K. Tiwary and S. Vasudevan, *Phys. Rev. B* **56**, 7812 (1997).
- [33] Z. P. Yin, K. Haule, and G. Kotliar, *Nature Mater.* **10**, 932 (2011).
- [34] G. Wagner and S. Friedberg, *Phys. Lett.* **9**, 11 (1964).
- [35] G. Rushbrooke and P. J. Wood, *Mol. Phys.* **1**, 257 (1958).
- [36] S. Emori, M. Inoue, M. Kishita, and M. Kubo, *Inorg. Chem.* **8**, 1385 (1969).
- [37] L. J. de Jongh and A. R. Miedema, *Adv. Phys.* **23**, 1 (1974).
- [38] M. Collins and O. Petrenko, *Can. J. Phys.* **75**, 605 (1997).
- [39] H. Forstat, N. Love, and J. McElearney, *Phys. Rev.* **139**, A1246 (1965).
- [40] C. Krellner, N. Caroca-Canales, A. Jesche, H. Rosner, A. Ormeci, and C. Geibel, *Phys. Rev. B* **78**, 100504 (2008).
- [41] “Inorganic Crystal Structure Database (ICSD), <https://icsd.fiz-karlsruhe.de/search/>,” .